



Enhanced Wear Resistance of Cobalt Oxide Over Nickel Oxide

Amit Roy^{1,2} · Vahid Jalilvand¹ · Saeed Mohammadkhani³ · Payank Patel^{1,2} · Ali Dolatabadi⁴ · L. Roue³ · D. Guay³ · Richard R. Chromik² · Christian Moreau¹ · Pantcho Stoyanov⁵

Received: 6 June 2023 / Accepted: 16 July 2023 / Published online: 29 July 2023
© The Author(s), under exclusive licence to Springer Science+Business Media, LLC, part of Springer Nature 2023

Abstract

Oxide-based coatings are being extensively investigated as potential solutions for high-temperature solid lubrication owing to their high thermal and chemical stability. Therefore, this study aimed to investigate the tribological behavior of the thermally sprayed CoO and NiO coatings. The dry sliding wear tests were conducted against the alumina counterface at room and high temperatures using a ball-on-flat tribometer. The results revealed that the friction and wear of CoO coatings decreased with increasing temperatures, while the NiO coatings showed opposite behaviors. *Ex situ* (SEM/FIB, XPS) analysis revealed that the formation of thin amorphous nanocrystalline tribofilm decreased friction and wear at high temperatures. On the other hand, NiO's high friction and wear at high temperatures were caused by the worn-out coatings, while at room temperatures, it showed the existence of brittle, cracked, and detached tribofilm on the wear track.

Keywords CoO · NiO · Thermal spray · Glaze layer · Tribology

1 Introduction

The performance of mechanical systems or machineries operating in demanding environments (e.g., power generation, transportation, materials processing, and aircraft engines) is often limited by the tribological behavior of employed materials and coatings [1–5]. Co and Ni-based

superalloys are widely used in high-temperature tribological applications due to their excellent strength, creep, and fatigue resistance at high temperatures [6–10]. Additionally, these alloys generate wear debris during sliding, which oxidize, and sinter/consolidate within the contacting interfaces forming the so-called “glaze” layer and consequently reducing the wear [3, 11, 12]. However, this glaze/oxide formation is affected by various factors, including temperatures, sliding speed, applied load, the chemical nature of surfaces. [13–15]. Dellacorte et al. [16] showed that a substantial reduction in friction appeared due to the formation of lubricious oxide layers when Co-based superalloy (i.e., Haynes 188) was sliding against Pt-coated MoRe at ~500 °C. A similar observation was observed by Coskun et al. [17], who found that Co-based superalloys (i.e., Haynes 25, Haynes 188, Haynes 214) form Co oxides protective layer along with Ni, Cr, and W oxides against Hastelloy X at 540 °C in sliding process. The process of glaze layer formation, spallation, and reformation by the load-bearing oxides during the sliding of Stellite 6 at 600 °C was analyzed by Wood et al. [12]. The authors identified six stages of wear: (i) mixed oxide glaze formation, (ii) Co and Cr diffusion to the glaze layer and hence forming Co and Cr-dominated oxide layers, (iii) oxygen diffusion to the glaze, (iv) spallation of the glaze, (v) reformation of the glaze, and (vi) elemental diffusion within the glaze. Similarly, Inman et al. [7, 8] demonstrated

✉ Amit Roy
amit.roy@concordia.ca

Richard R. Chromik
richard.chromik@mcgill.ca

Christian Moreau
christian.moreau@concordia.ca

Pantcho Stoyanov
pantcho.stoyanov@concordia.ca

¹ Department of Mechanical, Industrial and Aerospace Engineering, Concordia University, Montreal, Canada

² Department of Mining and Materials Engineering, McGill University, Montreal, Canada

³ INRS- Énergie, Matériaux, Télécommunications, 1650 Bd. Lionel Boulet, Varennes, QC J3X 1P7, Canada

⁴ Department of Mechanical and Industrial Engineering, University of Toronto, Toronto, ON M5S 3G8, Canada

⁵ Department of Chemical and Materials Engineering, Concordia University, Montreal, Canada

the effect of sliding on glaze layer formation at 750 °C for Nimonic 80A against Stellite 6. It was shown that low speed sliding (i.e., 0.314 m/s) resulted in the rapid development of a wear-resistant nano-structured Co/Cr/Ni oxide layer. In contrast, high speed sliding (i.e., 0.905 m/s) caused the formation of abrasive NiO and Cr₂O₃ debris. Furthermore, the authors concluded that lack of retention of a high amount of oxides led to loose abrasive wear debris and an increase in wear rate. In addition, Viat et al. [18] and Korashy et al. [19] showed cracks and a brittle nature of tribologically induced cobalt oxides glaze layer on Haynes 25 up to 200 °C, which increased the friction and wear coefficient. A similar behavior has been recently observed by Munagala et al. [20] for their HVOF-sprayed Diamalloy 3001 coatings up to 350 °C. They authors noticed the formation of cavity/cracks on the oxides tribolayer, and eventually, detachments of that layer led to an increment of wear rate at high temperatures. While the formation of mixed oxides on the wear tracks during sliding has shown to reduce the friction and wear for Co-based alloys, researchers claimed that a significant contribution comes from the cobalt oxides glaze layer [21–24]. In addition, more detailed analysis has previously revealed that this cobalt oxide glaze layer is nanocrystalline [11, 13, 25] and some studies emphasized the presence of amorphous zones near the surface [13, 26]. Similar results were also reported by Alixe et al. [27]. The authors showed that a thin 20 nm amorphous layer was present above the cobalt oxide glaze layer closer to the contacting interfaces, which improved the tribology of the Co-based alloy.

Similarly to Co-based alloys, Stott et al. [3] showed that the friction coefficient of nickel-based superalloys (i.e., Nimonic 75, Nimonic C263, Nimonic 108, and Incoloy 601) is reduced at high temperature (i.e., from 200 °C to 800 °C). This friction reduction could be due to the sintering of debris particles and formation of protective oxide (i.e., NiO, CoO, FeO, Cr₂O₃, NiCr₂O₄) layers on the wear track. In a similar study on nickel-based alloys, Laskowski et al. [28] observed the oxidation of the alloys at high temperatures (i.e., 500 °C and 800 °C). It was shown that the Inconel X-750 vs Rene 41 had the lowest friction coefficient (0.27) at 800 °C. In contrast, the Inconel X-750 vs Inconel 909 showed the lowest pin wear (i.e., 2.84×10^{-6} mm³/N-m) at 500 °C due to the formation of tenacious and lubricious oxide (i.e., Ni–Cr oxide) film on the wear tracks.

Thus, the formation of oxides in the contacting interfaces of the cobalt and nickel-based superalloys has been shown to reduce friction and wear, with the main constituent oxides being cobalt oxide and nickel oxide. These oxides play a significant role on the tribological properties at different temperatures, as first predicted by Peterson et al. [29]. The authors studied the frictional behavior of sintered cobalt and nickel oxides at different temperatures and showed that the cobalt oxide has improved lubricity compared to nickel

oxide, even though they have similar rock salt crystal structure and ionic potential. However, it still remains unclear on what the driving mechanism is behind the difference in frictional behavior between the CoO and NiO.

The main purpose of this study is to critically evaluate the friction and wear behavior of thermally sprayed CoO and NiO coatings at room temperature and high temperature. Emphasis is placed on providing a better understanding on the mechanisms behind the lubricating behavior. To the best of the author's knowledge, there is no data available on the tribological behavior of pure CoO and NiO coatings produced by such a thermal spraying process.

2 Experimental

CoO and NiO coatings were produced using HVOF and SPS, respectively. The HVOF process permits depositing the particles at a higher velocity and low in-flight temperatures, which allows for forming a dense coating with limited porosity [30]. NiO coatings were produced using SPS (Mettech, Canada) due to the lack of availability of larger particle sizes necessary for producing coatings using HVOF. However, the SPS process also allows the formation of coatings with thin splats on the substrate, which can be beneficial for wear resistance applications [31]. The substrate preparation for spraying, powder morphology, and particle size details can be found in previously published articles [32, 33]. Moreover, the details of the working principle of the HVOF and SPS process can be found in previously published literature by the authors and co-authors [30, 34–36]. The spraying parameters of CoO and NiO coatings are explained in Table 1.

According to standard metallographic guidelines, the as-sprayed coatings were cold-mounted and polished to a final

Table 1 Thermal spraying parameters used for depositing CoO and NiO coatings

Deposition parameters	(HVOF) values	(SPS) values
Oxygen flow	217 lpm	–
Propylene flow	70 lpm	–
Air flow	167 lpm	–
Total gas flow	–	180 lpm
N ₂ carrier gas flow	15 lpm	–
Ar gas flow rate	–	45%
N ₂ gas flow rate	–	45%
H ₂ gas flow rate	–	10%
Current	–	180 amps
Power	–	78 kW
Feed rate	10 gm/min	45 ml/min
Spray distance	180 mm	50 mm
Number of passes	55	80

surface finish of 0.4 μm . The top surface and cross-section of the HVOF and SPS sprayed CoO and NiO coatings were analyzed using scanning electron microscopy (SEM). Likewise, the chemical composition was determined by energy-dispersive X-ray spectroscopy (EDS).

Dry sliding wear tests on the coatings were performed using a reciprocating ball-on-flat tribometer (Anton Paar TriTec SA, Switzerland). The details of the friction testing parameters (i.e., applied load of 5N, track length of 10 mm, and total sliding cycles of 5000) were adopted from the previously published article [30]. The friction testing parameters were selected based on the conditions of moving mechanical assemblies [30]. An alumina (McMaster-Carr, USA) ball with a diameter of 6.35 mm was used as the counterface. The wear testing was performed on the as-sprayed coatings (i.e., without further polishing the top surfaces of the coatings) at two different temperatures: room or atmospheric temperature (RT), and high temperature (HT). For the high-temperature (HT) testing, the samples (substrate/coating) were placed in the furnace, where they were heated to 450 $^{\circ}\text{C}$. The temperature recorded on the surface of the coating was around 300 $^{\circ}\text{C}$ (i.e., using a thermocouple). In this study, the atmospheric and high temperatures friction testing conditions were denoted as RT and HT, respectively. Here, it can be mentioned that friction testing was also performed on the polished coatings (not shown here), but no huge significant changes in the friction results were noticed. Thus, further characterization was carried out on the as-sprayed coating wear tracks. The main motive behind choosing as-sprayed conditions was to make it applicable in practical applications without performing additional surface finishing processes, which will reduce the lead time and cost of the overall component. The consistency of the wear tests was checked by performing three repeats. The depth of wear tracks and wear volume of counterface alumina was measured using a 3D optical surface profiler (Zygo Corporation, USA). The wear area (mm^2) was calculated by integrating the wear track profiles, and the wear area was multiplied by track length (mm) to determine the wear volume (mm^3). The

wear volume was normalized by dividing with applied load (N) and total sliding distance (m) to obtain the specific wear rate, k ($\text{mm}^3/\text{N.m}$.), as per the equation below [37].

$$k = \frac{V}{d.w} \quad (1)$$

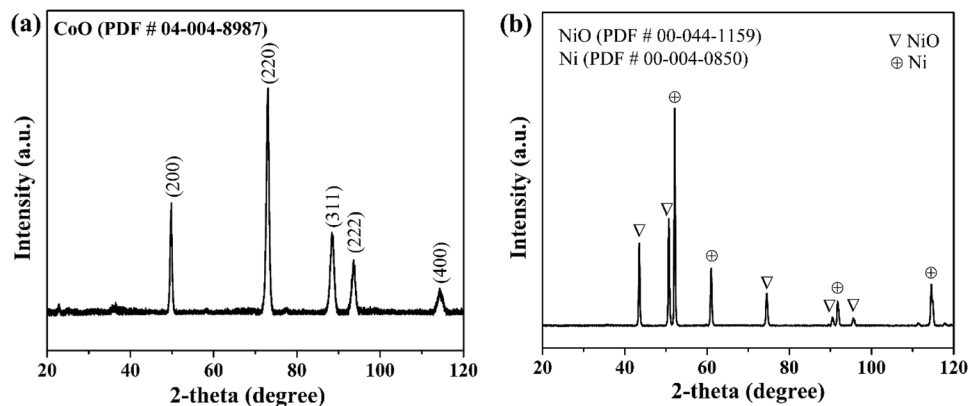
where V = volume loss (mm^3), d is the total sliding distance (m), and w is the applied load (N).

To characterize the phases after tribological testing, Raman analysis was performed using an InVia spectrometer (Renishaw, UK) on the unworn and worn coatings with an Ar^+ ion ($\lambda = 514.5$ nm) laser source. The obtained Raman shift was matched with published literature data.

In order to reveal wear mechanisms, Focus Ion Beam Scanning (FIB) (FEI Helios 600 NanoLab 660, Thermo Fisher Scientific, USA) was also used to cut the specific position of the worn surface of CoO wear tracks. A Ga/Pt thin layer was deposited on the wear tracks to protect the surface. An electron channeling contrast imaging (ECCI) was performed on this FIB cut to see the grain refinement and structure. ECCI on the wear tracks cross-sections was performed using a cold field emission SEM (SU8230, Hitachi, Japan) fitted with a photodiode BSE detector. Moreover, worn surfaces and manual cross-sections of wear tracks of NiO coatings were examined using an SEM equipped with energy-dispersive X-ray spectroscopy (EDS).

An X-ray photoelectron spectroscopy (XPS) was performed on as-sprayed CoO coatings and wear tracks after sliding tests at RT and HT with a VG ESCALAB 250 Xi (Thermo VG Scientific) Al K_{α} X-ray source set to 14 kV and 218 W. The coating's atomic concentration and chemical/oxidates states were evaluated with this XPS analysis.

Fig. 1 XRD pattern of coatings prepared from **a** CoO and **b** NiO powder



3 Results

3.1 Coating Characteristics

The XRD graphs of thermally sprayed CoO and NiO coatings are shown in Fig. 1. The diffraction peaks associated with 49.77° (200), 73.03° (220), 88.49° (311), 93.57° (222), and 114.6° (400) can be indexed to Powder Diffraction File (PDF) 04-004-8987 for CoO [Fig. 1a]. The NiO powder was partially reduced into metallic Ni for NiO coating [Fig. 1b]. The diffractions peaks (i.e., 43.54° (101), 50.72° (012), 74.53° (110), 90.50° (113), 95.90° (006)) for NiO and Ni (i.e., 52.18° (111), 61.02° (200), 91.76° (220), 114.69° (311)) matched with PDF 00-044-1159, and PDF 00-004-0850, respectively. The reduction of the NiO into pure Ni could be due to the presence of hydrogen gas during spraying, which can be explained using the Ellingham diagram [38, 39]. The different conditions/reasons for reducing NiO into metallic Ni have been previously described by co-authors elsewhere [33, 40].

SEM cross-sections of the CoO and NiO coatings are shown in Fig. 2a, and b, respectively. The CoO coating revealed a denser microstructure which can possibly attributed to the high velocity of the in-flight particles of the HVOF process [30] [Fig. 2a].

On the other hand, an irregular surface with cauliflowers (not shown here) has been observed on the surface of

the NiO coatings. The presence of pores (red circle) and metallic Ni (yellow arrows) in the NiO coatings is shown in [Fig. 2b]. These results were further confirmed by the line scans on the coatings shown in Fig. 3. The high intensity on white zones indicated Ni, whereas the grey contrast showed the homogenous distribution of Ni and O, proving the NiO phase [Fig. 3]. The details of the coating's surface morphology and microstructures of CoO and NiO were described elsewhere [32, 33].

3.2 Sliding Wear Behavior

3.2.1 Coefficient of Friction and Specific Wear Rate

The coefficient of friction vs number of cycles of CoO and NiO coatings is shown in Fig. 4. The coefficient of friction of the CoO and NiO coatings behaved quite differently at both, room temperature (RT) and high temperature (HT). At RT, the friction coefficient of the CoO and NiO was 0.63 and 0.45, respectively. On the other hand, at HT, the friction value of CoO decreased to 0.5, whereas NiO's friction coefficient increased (i.e., 0.7) up to 500 cycles and then dropped to 0.5. The sudden reduction of the friction coefficient of NiO at HT was due to the wear out of the coatings. In order to confirmed that further sliding wear testing was performed on NiO coating up to 500 and 1000 cycles at HT. It was found that the coatings worn out after 500 cycles which was verified by finding substrate elements (i.e., Fe, Cr, Mn, Si)

Fig. 2 SEM cross-section of **a** CoO and **b** NiO coating (Color figure online)

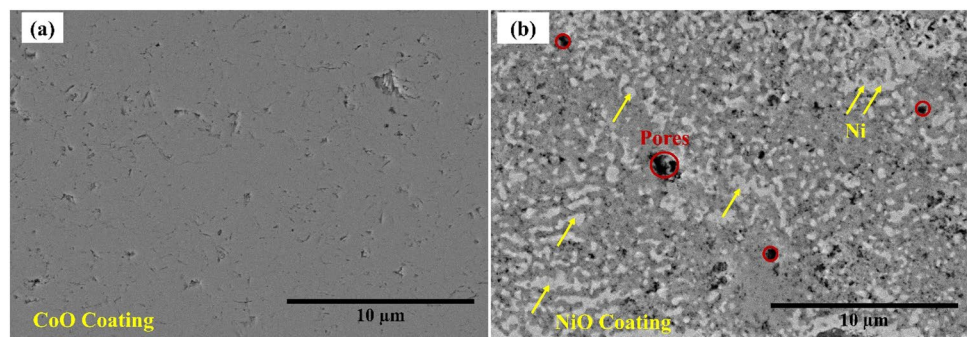


Fig. 3 Cross-sectional SEM line scan of NiO coating, showing the distribution of NiO and metallic Ni (Color figure online)

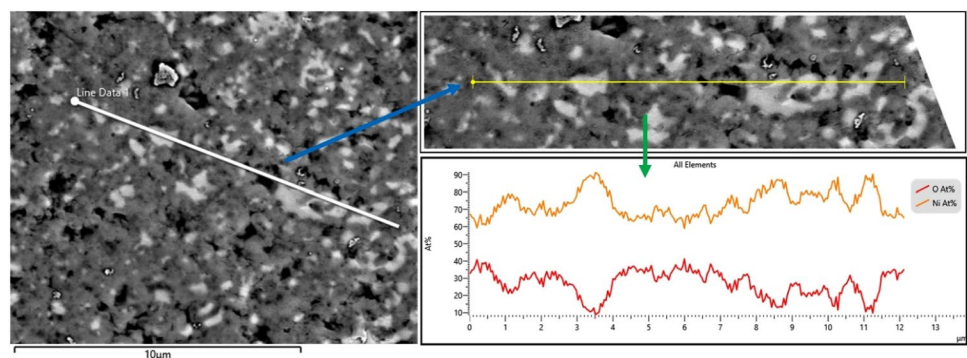


Fig. 4 Friction coefficient vs no. of cycle of CoO and NiO coatings at room (RT) and high temperature (HT)

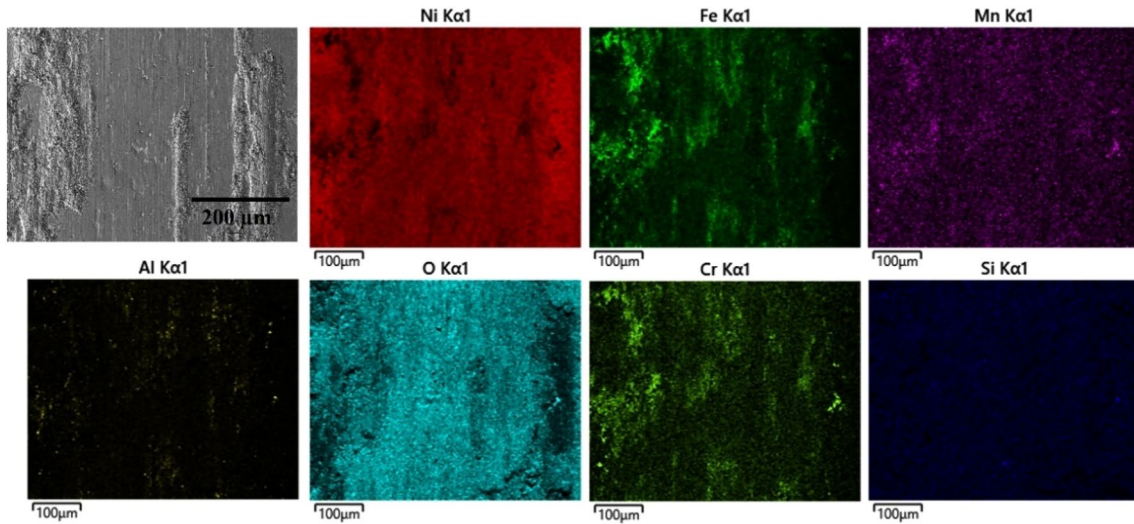
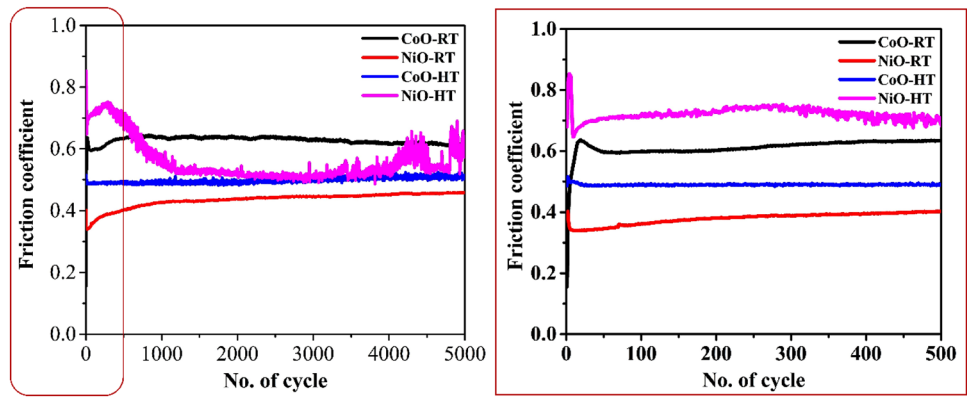


Fig. 5 SEM-EDS mapping of wear track after sliding 500 cycles at high temperature (HT) on the NiO coating

using the SEM/EDS mapping on the worn surfaces [Fig. 5]. Furthermore, a small fraction of Al was found on the wear tracks which was from counterball Al_2O_3 [Fig. 5]. However, the friction coefficient of CoO and NiO at RT and CoO at HT maintained a steady state in all conditions except in the first few cycles, which could be due to the asperity polishing during sliding [41].

The specific wear rate of CoO and NiO coatings at RT and HT is shown in Fig. 6. The wear rate of CoO at RT and HT was $22 \pm 2.4 \times 10^{-6} \text{ mm}^3/\text{Nm}$ and $12 \pm 2.0 \times 10^{-6} \text{ mm}^3/\text{Nm}$, respectively. On the other hand, NiO wear rate ($42 \pm 6.04 \times 10^{-6} \text{ mm}^3/\text{Nm}$) was more than 45% higher than CoO at RT. The NiO coating has also worn out at high temperatures after the sliding test. Therefore, the wear rate at this temperature was relatively high and not depicted in Fig. 6 but mentioned as ‘coating worn out’.

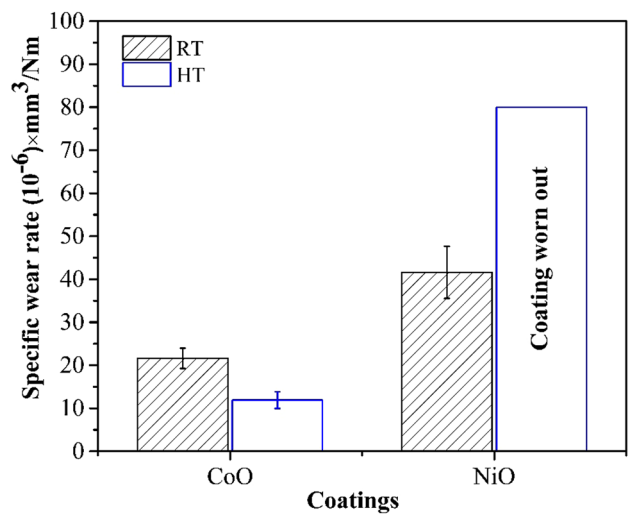
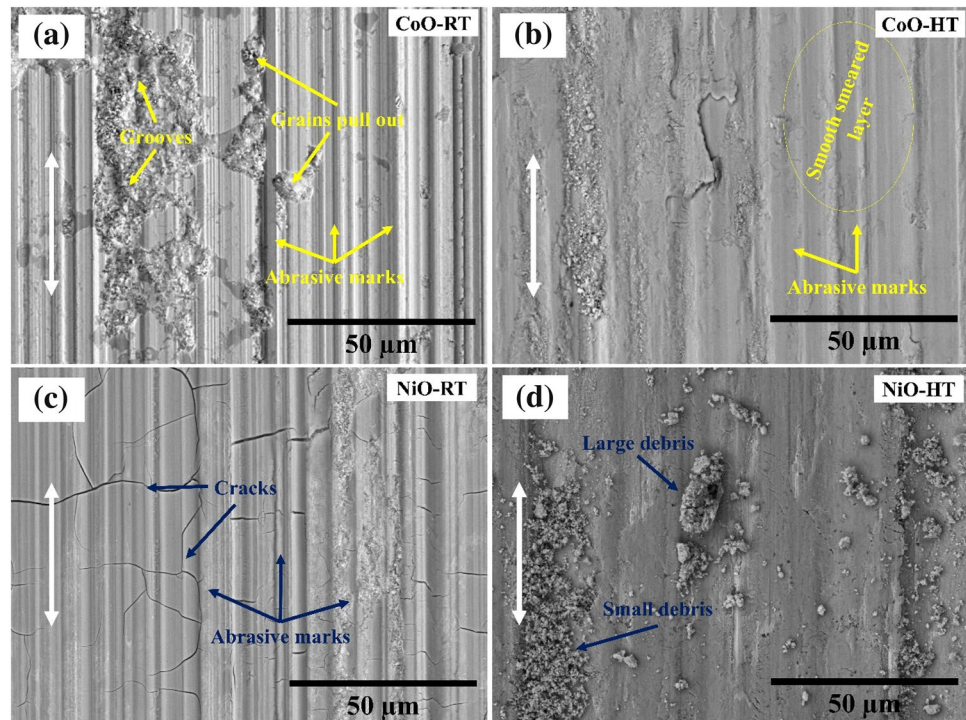


Fig. 6 Specific wear rate of CoO and NiO coatings at room (RT) and high temperature (HT)

Fig. 7 SEM micrograph of the wear tracks after dry sliding test of **a** CoO at RT, **b** CoO at HT; **c** NiO at RT and **d** NiO at HT. \updownarrow indicate sliding directions



3.2.2 Worn Surface Morphologies

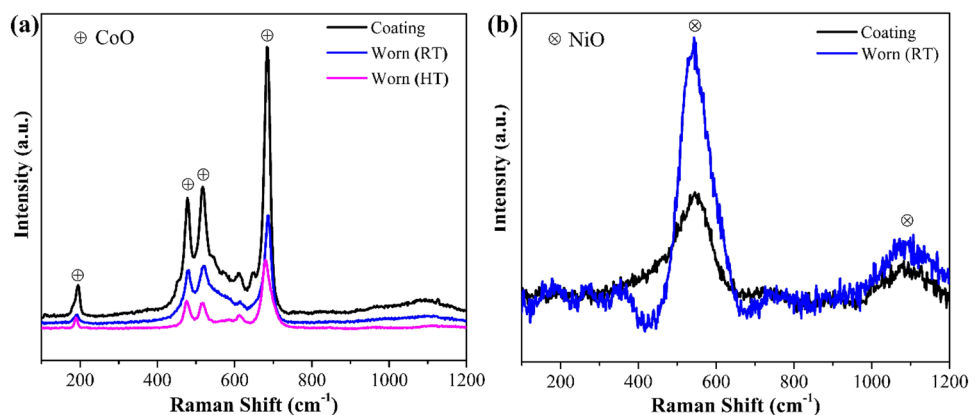
Figure 7 shows the SEM wear tracks of the CoO and NiO coatings after the dry sliding tests at RT and HT. Figure 7a shows the deep abrasive mark along the sliding direction with some grooves or grain pull out on the wear tracks. The grain pull-outs were mainly found in the ceramics where the boundaries of the surface grains were weaker and hence removed as the wear debris during sliding [42]. It should be noted that most of the wear debris are likely generated at the beginning of the testing due to the removal of the asperities. At HT, a comparatively smooth smeared surface with some shallow abrasive marks was observed on the worn surfaces [Fig. 7b].

Abrasive lines/grooves parallel to the sliding direction for the NiO coatings was observed at RT [Fig. 7c]. Additionally, fracture, and/or cracks propagated on the wear tracks perpendicular to the sliding direction or at a slight angle. On the contrary, the NiO coatings wore out after sliding at 5000 cycles at HT. The size of the debris particles varied between a few micrometers and the composition is a mixture between the substrate (i.e., steel) elements and the coating (not shown here). This behavior indicated the low load-carrying capacity or poor wear resistance properties of NiO coatings at HT.

3.2.3 Raman Analysis

Raman analysis was performed on the deposited coatings and worn surfaces (i.e., CoO and NiO) after sliding at RT

Fig. 8 Raman spectrum of unworn and worn coatings at **a** room temperature (RT) and **b** high temperature (HT)



and HT (except wear track of NiO at HT as it worn out) as shown in Fig. 8. The micro-Raman analysis on the CoO and NiO coatings correlated well with the XRD analysis [Fig. 1]. However, pure metallic Ni in the NiO coating [Fig. 1b] was not detected with the Raman spectrum [Fig. 8b] as it is not Raman active.

The characteristic peaks at Raman shift 190 cm^{-1} , 477 cm^{-1} , 516 cm^{-1} and 680 cm^{-1} in the unworn, worn coatings at RT and HT corresponding to the CoO phase [Fig. 8a] [43, 44]. The peaks at Raman shift 545 cm^{-1} and 1080 cm^{-1} corresponds to NiO phase [Fig. 8b] [43, 45].

3.2.4 Counterface Analysis

3.2.4.1 Counterface Against CoO Coating SEM images of the Al_2O_3 counterball running against CoO are shown in Fig. 9 after sliding testing at RT and HT. The RT counterball shows material transfer on the center and periphery of the contact [Fig. 9a]. In addition, the SEM image [Fig. 9a, b] depicted severe abrasive marks in the sliding direction with materials island covering parts of the grooves. This severe abrasive behavior of the counterball is similar to that observed on the wear tracks at RT [Fig. 7a]. A similar behavior was also observed for the HT counterball [Fig. 9c, d]. However, the abrasive grooves were less evident, which correlates well with the wear tracks at HT Fig. 7b. The wear of the counterballs Al_2O_3 was observed after dry sliding at RT (i.e., $0.65 \pm 0.02 \times 10^{-6}\text{ mm}^3/\text{Nm}$) and HT (i.e., $0.67 \pm 0.002 \times 10^{-6}\text{ mm}^3/\text{Nm}$) was almost the same as illustrated in Table 2.

Table 2 Wear rate of Al_2O_3 counterface against CoO and NiO coatings at RT and HT after dry sliding wear testing

Coating	Testing condition	Counterface wear rate $\times 10^{-6}$ (mm^3/Nm)
CoO	RT	0.65 ± 0.02
	HT	0.67 ± 0.002
NiO	RT	1.20 ± 0.02
	HT	15.32 ± 0.6

3.2.4.2 Counterface Against NiO Coating The Al_2O_3 counterfaces sliding against the NiO coatings at RT and HT are shown in Fig. 10. Severe abrasive grooves with transferred material in the centre of the contact can be observed at RT counterfaces [Fig. 10a, b]. The abrasive behavior could possibly be due to the abrasive nature of the NiO debris particles that formed on the wear tracks at RT [Fig. 7c]. On the other hand, a vast and thick transfer film mixed with NiO and steel elements (not shown here) in the center and edges of the contact has been observed at HT counterfaces [Fig. 10c, d]. This thick transfer is likely due to the worn-out of the NiO coatings after the sliding test at HT [Fig. 7d]. On the other hand, the wear on the alumina counterface at RT (i.e., $1.2 \pm 0.02 \times 10^{-6}\text{ mm}^3/\text{Nm}$) was low than HT but substantially higher than counterfaces sliding against CoO coatings [Table 2].

Fig. 9 SEM microstructures of Al_2O_3 counterfaces sliding against CoO coatings at **a, b** room temperature (RT), and **c, d** high temperature (HT)

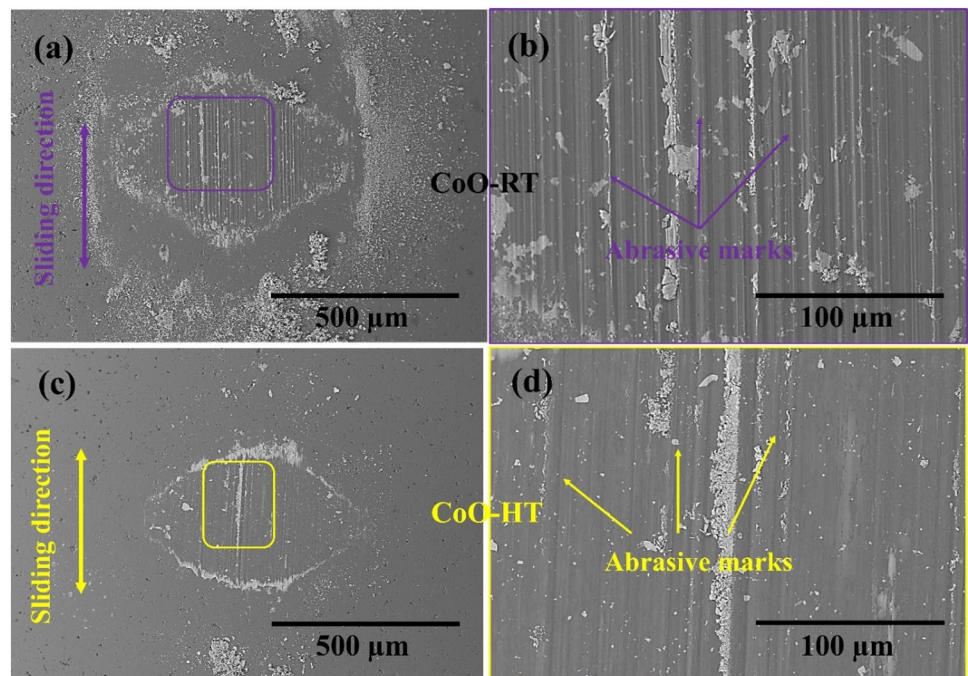
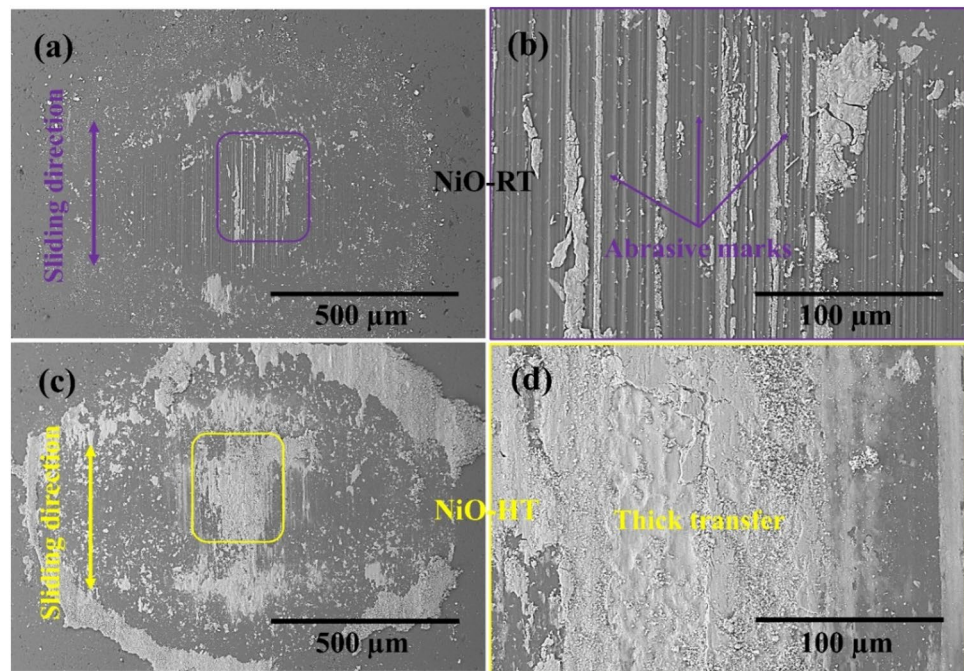


Fig. 10 SEM microstructures of Al_2O_3 counterfaces sliding against NiO coatings at **a, b** room temperature (RT), and **c, d** high temperature (HT)



3.2.5 Subsurface microstructure

3.2.5.1 CoO Subsurface Analysis The material's properties and microstructures in the subsurface (i.e., underneath the wear track) is generally modified during sliding in demanding conditions due to stress transfer or contact conditions during sliding, influencing the friction and wear mechanisms [20, 46]. Thus, FIB/SEM analysis was performed on the wear tracks (preferably on the smoother zones) developed at RT and HT to characterize the subsurface microstructures. Figure 11a and d shows the Focused Ion Beam (FIB)-SEM images in low magnification at RT and HT, respectively. The high-magnification ECCI images at RT are shown in Fig. 11b and c, which clearly reveal submicrometric grains throughout the micrographs. No apparent tribofilm or grain refinement was observed near the contact interfaces. In addition, crack propagation and/or fractures appeared below the worn surface (i.e., closer to contact interfaces). Interestingly, three (I, II & III) distinct zones along with sintered or compacted grains can be seen in the ECCI cross-section of the wear track at HT [Fig. 11e, f]. Zone I is associated with the nanocrystalline/amorphous layer on the surface, zone II is the nanocrystalline zone underneath, and zone III is the sub-micrometric zone.

EDS mapping and line analysis were performed on the CoO wear tracks to distinguish the variation of Co and O [Fig. 12]. Co and O were distributed homogeneously on the sub-surface without any variation. This was an initial indication that the only structural modifications (i.e., grain refinement) of the coatings in the sub-surface occurred during sliding at HT [Fig. 11e, f].

The x-ray photoelectron spectroscopy (XPS) showed no significant variation of Co and O elements in the coatings and the wear tracks at RT [Fig. 13a, b]. However, HT wear tracks showed a variation of Co and O on the surface and remained similar as a function of depth [Fig. 13c]. The Co and O elements on the HT wear track could be associated with Co_3O_4 .

3.2.5.2 NiO Subsurface Analysis The cross-section of the NiO coating after wear testing at RT is shown in Fig. 14. It should be noted that the cross-section of the NiO wear track at HT is not shown here since it was completely worn out after friction testing.

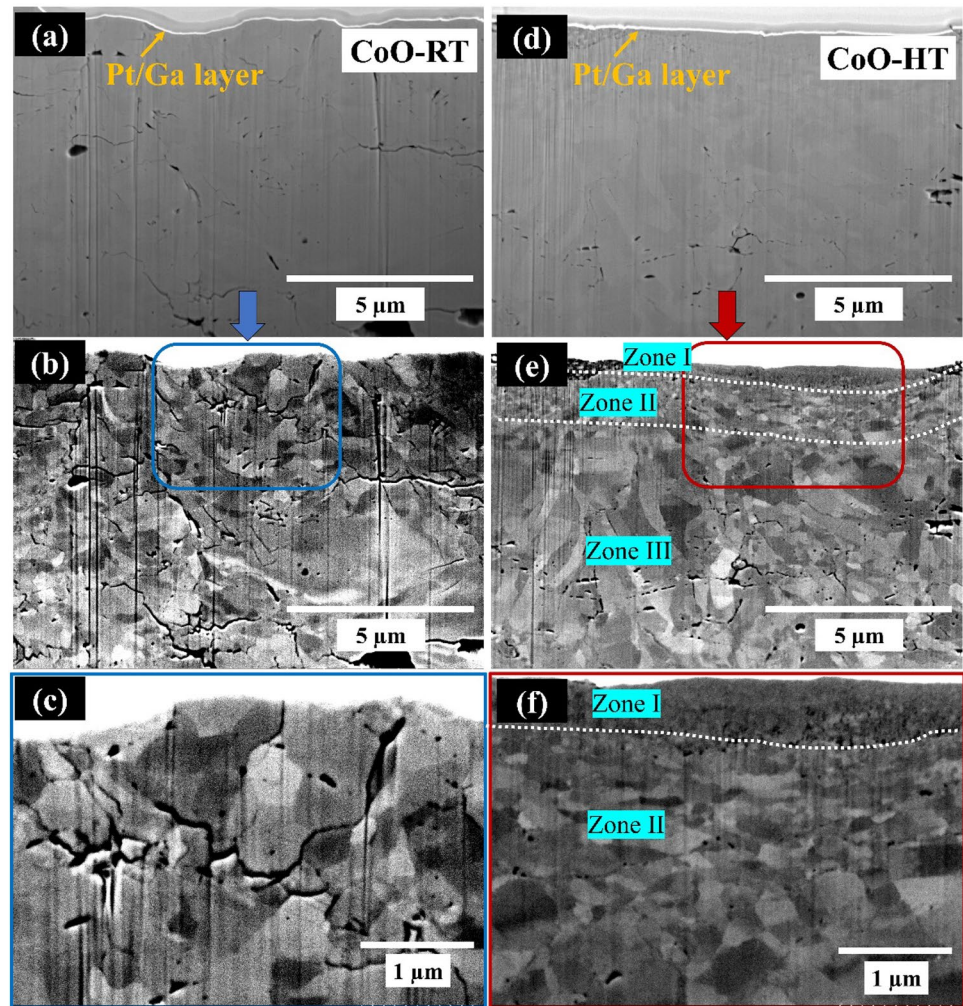
A dense layer (i.e., tribofilm) at RT was formed on the wear tracks, as shown in Fig. 14a, which can be associated with cracks, brittle fractures, and spallation from the coating [Fig. 14b, c]. The cracks (i.e., yellow circles) within the tribolayer are consistent with the cracks observed on the surface of the wear tracks Fig. 7c. These characteristics can be related to the hard and brittle behavior of the tribolayer [47–49].

4 Discussion

4.1 Friction and Wear Mechanisms of CoO Coatings

In order to provide a better understanding on the friction and wear mechanisms of CoO coatings sliding at RT and HT, a schematic is shown in Fig. 15 based on the *ex situ* analysis performed in this study. At room temperature, the governing

Fig. 11 SEM/FIB image of CoO coatings at **a** room temperature (RT) and **d** high temperature (HT). ECCI micrograph of this FIB cut of CoO wear track at **b, c** RT and **e, f** HT; **Zone I**: nanocrystalline/amorphous layer, **Zone II**: nanocrystalline zone, and **Zone III**: sub-micrometric zone



wear mechanism is abrasion (i.e., possibly 2 or 3 body abrasions) with significant plastic flow of the asperities, which is indicated through the grooves in the parallel direction to the sliding, [Fig. 7a] [50]. In addition, it is likely that localized shear deformation occurred due to the cyclic exposure of the wear track. The cyclic loading and frictional heating in the contact zone at RT were not sufficient to change any sub-surface grain refinement and thus, sub-micrometric grains were observed throughout the sub-surface [Fig. 15a]. However, this cyclic loading led to the development of sub-surface cracks [Fig. 11b, c and Fig. 15a], detachment of materials from the worn surface, and formation of wear debris that accelerated severe abrasion, resulting in high friction and wear rates [Fig. 4 and Fig. 6]. Crack formation and brittle behavior of ceramics at room temperature could accelerate detachment of wear fragments during sliding, generate high wear debris, and cause increased friction and wear [41]. A similar formation of brittle cracks on the wear tracks has been observed on the tribologically induced cobalt oxides for Co-based alloys, which were previously reported by Viat et al. [18], Korashy et al. [19] and Munagala et al. [20]. Also,

Viat et al. [18] proved by micropillar compression testing that this oxides layer behaved as brittle behavior from room to 200 °C, which resulted in relatively high friction and wear rates at room temperatures.

At high temperature, a comparatively smooth smeared surface with some shallow abrasive marks was observed on the wear tracks [Fig. 7b]. The more ductile behavior in combination with the high frictional heating and reduced thermal conductivity (i.e., 9 W/m.K. at ~25 °C) at high-temperature environment could promote the formation of such a smeared smooth surface on the wear tracks [51]. Consequently, this smeared tribofilm on the wear tracks will result in a low and stable friction coefficient and high wear resistance characteristics at HT compared to RT [Figs. 4 and 6]. A similar observation of continuous smeared tribofilm was observed by Roy et al. [35] for their plasma-sprayed tantalum oxide coatings at elevated temperatures, which reduced friction and wear. Additionally, Viat et al. [18] showed that the tribologically induced cobalt oxides undergo the brittle to ductile transition at above 300 °C, which decreased friction and wear.

Fig. 12 EDS mapping and line analysis (i.e., top to bottom) of CoO at room temperature (RT) and high temperature (HT)

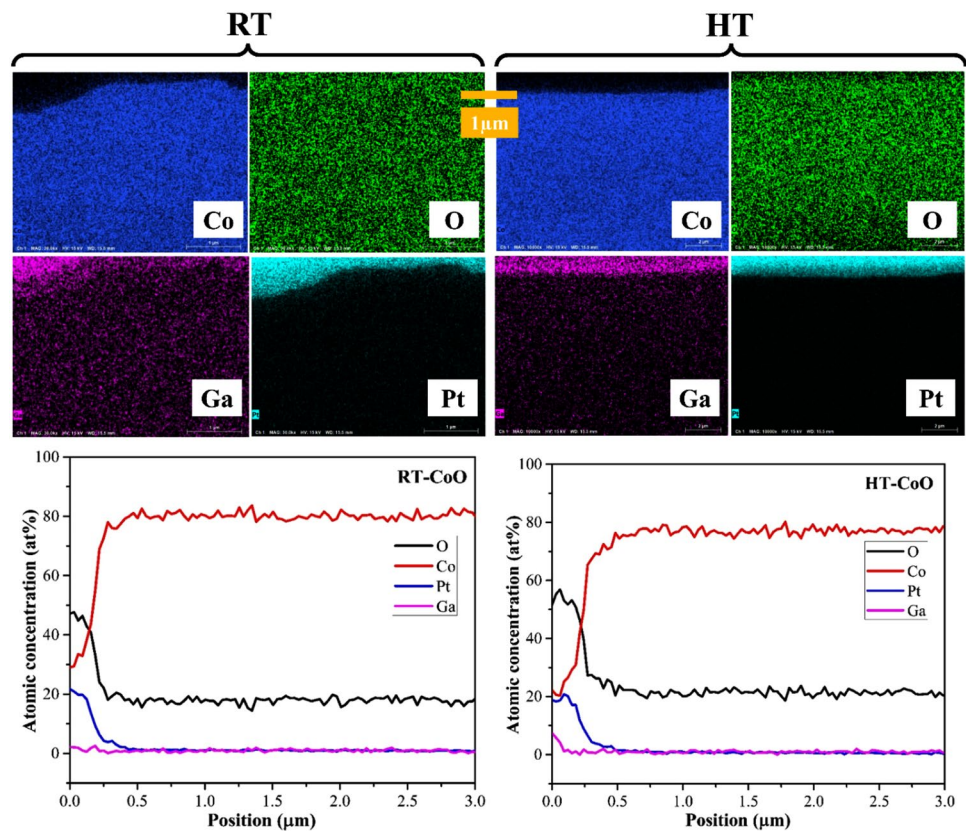
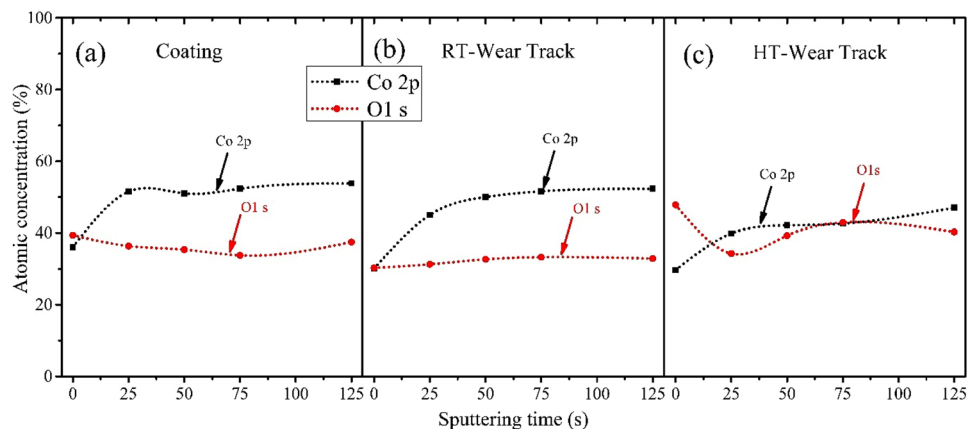


Fig. 13 XPS depth profiles of CoO **a** coating, **b** wear track at room temperature (RT), and **c** wear track at high temperature (HT)



This behavior could be responsible for changing the severe abrasive wear (RT) to mild abrasive wear at HT [Fig. 7b].

Three distinctive zones (i.e., nanocrystalline amorphous, nanocrystalline, and sub-micrometric) were identified in the sub-surface of HT wear tracks, as explained in Sect. 3.2.5. This is consistent with previous studies highlighting that the glaze layers closer to the interface were nanocrystalline with increased hardness for Co-based alloys, which ultimately decreased friction and wear [13, 15, 26, 52]. This behavior has also been observed in other metallic alloys, forming lubricious oxide glazes on the

wear tracks at high temperatures [20, 53, 54]. Some studies have even shown the presence of amorphous zones along with nanocrystalline grains in these cobalt oxide tribolayers [13, 26, 55]. In addition, Tang et al. [56] showed that the formation of CoO or Co₃O₄ oxides layer on the wear track at high temperatures can be explained by the greater diffusion of Co than Cr, which reduced the overall friction and wear for cobalt-based superalloys. The frictional heating at high temperatures could play a significant role for the formation of Co₃O₄ or remain CoO as per Eq. (2) [56]. Query However, further advanced characterization needs

to be performed to fully understand the type or nature of the tribofilm closer to the contact interfaces.

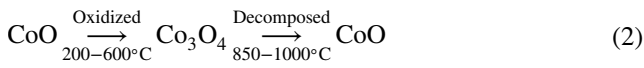
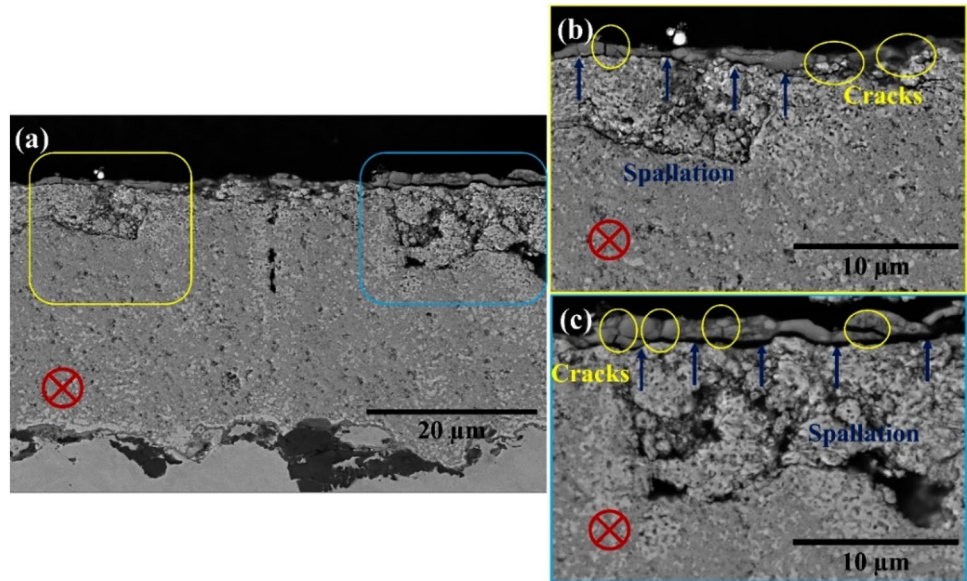


Fig. 14 SEM-cross-section of wear tracks of NiO coatings after tribotesting at room temperature (RT). Blue arrows and yellow circles showed spallation and cracks in the tribolayer. ⊗ indicate sliding direction (Color figure online)



4.2 Friction and Wear Mechanisms of NiO Coatings

Similar to CoO, a schematic (Fig. 16) of the friction and wear mechanisms for the NiO coatings at RT and HT is shown based on the *ex situ* analysis. The friction coefficient of NiO coatings was lower than the CoO coatings at RT [Fig. 4]. The low friction could be due to the high hardness of the NiO as compared to CoO coatings [57]. The effect of hardness on friction coefficient is described by

Fig. 15 Friction and wear mechanisms of CoO coatings after dry sliding at **a** room temperature (RT) and **b** high temperature (HT). ⊗ indicate sliding direction

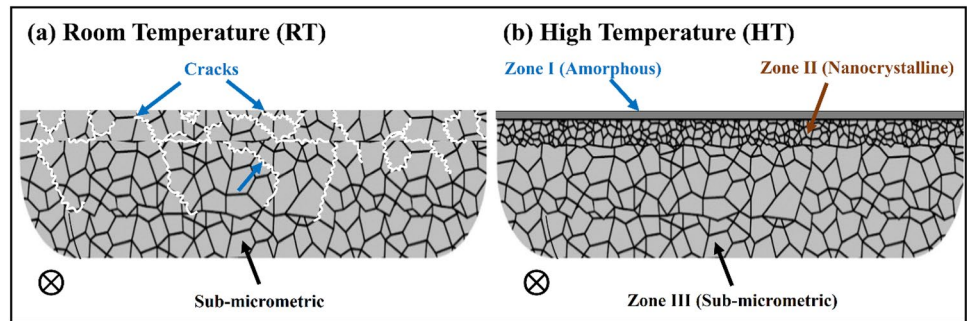
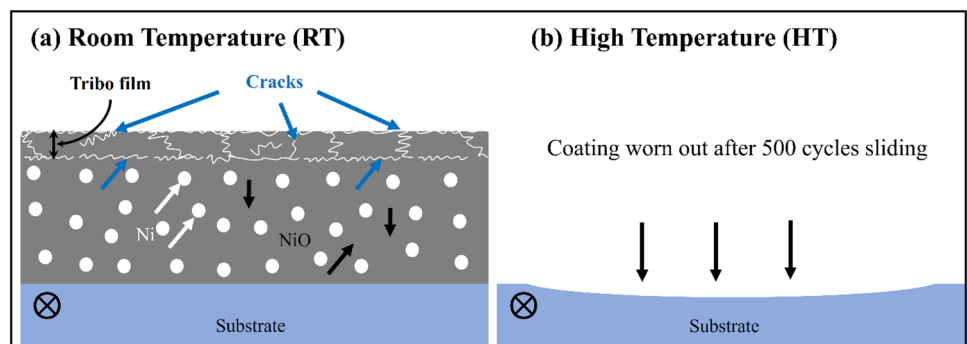


Fig. 16 Friction and wear mechanisms of NiO coatings after dry sliding at **a** room temperature (RT) and **b** high temperature (HT). ⊗ indicate sliding direction



the Archard [58]. Indeed, the high hardness coatings can significantly reduce friction, as observed by researchers in their previously published literature [59–62]. However, due to the brittleness of the NiO, cracks were propagated on the wear track while two or three body abrasive wear mechanisms was dominant [Figs. 7c and 16a]. Evans et al. previously showed NiO is hard and brittle in atmospheric conditions [63]. Consequently, the formation of cracks and brittle natures of ceramics accelerated the removal of wear fragments during sliding, generating high wear debris, and consequently high wear [41]. Goel et al. [46] and Mahade et al. [47] have observed a similar behavior in their plasma-sprayed alumina coatings at atmospheric sliding conditions.

At high temperature, the friction coefficient of NiO coating was relatively high (~0.7) up to 500 cycles, which could possibly be due to the generation of hard particles (i.e., NiO) in the sliding process. A similar explanation for the high friction of NiAl coatings at high temperatures was made by Yao et al. [45]. Similarly to the friction coefficient, the wear rate of NiO coatings was relatively high and the coating was completely removed at the end of the test [Fig. 6; Fig. 7d; Fig. 16b]. Evans et al. showed that NiO employs its brittle nature up to 500 °C [63]. Therefore, in our study, it is likely that the NiO coating failed prematurely due to brittle fracture within the worn area.

In general, the lubricity of the CoO and NiO at high temperatures can be related to the polarizability approach or interaction parameter [64, 65]. The interaction parameter of CoO and NiO are 0.059 and 0.083, respectively. Prakash et al. [65] found that with decreasing the interaction parameter the friction coefficient of the oxides decreased at high temperatures due to the weaker bond energy between anion and cation. In addition, the interaction parameter can be related to the activation energy for the improved lubricity. More specifically, the formation of vacancies and hopping of ions at the surface of an oxides becomes easier with lower the activation energy, and thus, increases the degree of freedom and mobility of ions. This increased mobility of ions at their surface is assumed to be at the basis of the low coefficient of friction of such oxides in sliding contacts [65].

5 Conclusions

The main purpose of this study was to critically evaluate the friction and wear behavior of the thermally sprayed CoO and NiO coatings at room temperature (RT) and high temperature (HT). In terms of wear characteristics, the CoO coatings outperform NiO in both states. The friction coefficient and specific wear rate of the CoO coatings decreased with increasing temperatures. *Ex situ* analysis of the wear tracks after sliding at high temperatures revealed the formation of a thin, nanocrystalline amorphous

tribofilm. At room temperature, brittle fractures, and sub-surface micro-cracks of CoO coating caused high friction and wear. At room temperature, NiO coating provided low friction and wear, which can possibly be attributed to the high hardness. At high temperature, on the other hand, the coating was utterly worn out and resulted in increased friction and wear due to its brittle nature [63].

Acknowledgements The authors thank the Natural Sciences and Engineering Research Council of Canada (NSERC) through the Strategic program (STPGP/494283-2016), Prima Quebec (Grant R13-13-001), Metal7, Kingston Process Metallurgy, and NSERC Discovery Grant-Pantcho Stoyanov for supporting this work financially.

Author Contributions AR: writing- original draft preparation, experiments, data analysis, reviewing and editing. VJ: experiments, critical review. SM: experiments, critical review. PP: experiments, critical review. AD: study conceptualization, reviewing and editing. LR: study conceptualization, reviewing and editing. DG: study conceptualization, reviewing and editing. RRC: supervision, funding acquisition, study conceptualization, data analysis, reviewing and editing. CM: supervision, funding acquisition, study conceptualization, data analysis, reviewing and editing. PS: supervision, funding acquisition, study conceptualization, data analysis, reviewing and editing.

Funding Natural Sciences and Engineering Research Council of Canada (NSERC) (STPGP/494283-2016), Prima Quebec (R13-13-001), Metal7, Kingston Process Metallurgy, and NSERC Discovery Grant-Pantcho Stoyanov.

Data Availability Data will be made available on request.

Declarations

Conflict of interest The authors declare that they have no known competing financial interests or personal relationships that could have appeared to influence the work reported in this paper.

References

1. Wood, P.D.: The effect of the counterface on the wear resistance of certain alloys at room temperature and 750 °C. University of Northumbria, Newcastle (1997)
2. Rose, S.R.: Studies of the high temperature tribological behaviour of some superalloys. University of Northumbria, Newcastle (2000)
3. Stott, F.H., Lin, D.S., Wood, G.C.: The structure and mechanism of formation of the 'glaze' oxide layers produced on nickel-based alloys during wear at high temperatures. *Corros. Sci.* **13**, 449–469 (1973)
4. Ross, E., Ignatov, A., Stoyanov, P.: Tribological characteristics of manufactured carbon under extreme contact conditions. *Tribol. Int.* (2021). <https://doi.org/10.2484/ti.968.09.20.06>
5. Stoyanov, P., Harrington, K.M., Frye, A.: Insights into the tribological characteristic of Cu-based coatings under extreme contact conditions. *JOM.* **72**, 2191–2197 (2020)
6. Korashy, A., Attia, H., Thomson, V., Oskooei, S.: Fretting wear behavior of cobalt-based superalloys at high temperature—a comparative study. *Tribol. Int.* **145**, 106155 (2020)
7. Reed, R.C.: The superalloys: fundamentals and applications. Cambridge university press (2008)

8. Stoyanov, P., Dawag, L., Goberman, D.G., Shah, D.: Friction and wear characteristics of single crystal Ni-based superalloys at elevated temperatures. *Tribol. Lett.* **66**, 1–9 (2018)
9. Pollock, T.M., Tin, S.: Nickel-based superalloys for advanced turbine engines: chemistry, microstructure and properties. *J. Propuls. power.* **22**, 361–374 (2006)
10. Stoyanov, P., Dawag, L., Joost, W.J., Goberman, D.G., Ivory, S.: Insights into the static friction behavior of Ni-based superalloys. *Surf. Coatings Technol.* **352**, 634–641 (2018)
11. Inman, I.A., Datta, S., Du, H.L., Burnell-Gray, J.S., Luo, Q.: Microscopy of glazed layers formed during high temperature sliding wear at 750 °C. *Wear* **254**, 461–467 (2003)
12. Wood, P.D., Evans, H.E., Ponton, C.B.: Investigation into the wear behaviour of Stellite 6 during rotation as an unlubricated bearing at 600 C. *Tribol. Int.* **44**, 1589–1597 (2011)
13. Viat, A., Bouchet, M.-I.D.B., Vacher, B., Le Mogne, T., Fouvry, S., Henne, J.-F.: Nanocrystalline glaze layer in ceramic-metallic interface under fretting wear. *Surf. Coatings Technol.* **308**, 307–315 (2016)
14. Viat, A., Dreano, A., Fouvry, S., Bouchet, M.-I.D.B., Henne, J.-F.: Fretting wear of pure cobalt chromium and nickel to identify the distinct roles of HS25 alloying elements in high temperature glaze layer formation. *Wear* **376**, 1043–1054 (2017)
15. Viat, A., Guillonneau, G., Fouvry, S., Kermouche, G., Sao Joao, S., Wehrs, J., Michler, J., Henne, J.-F.: Brittle to ductile transition of tribomaterial in relation to wear response at high temperatures. *Wear* **392**, 60–68 (2017)
16. DellaCorte, C., Lukaszewicz, V., Morris, D.E., Steinetz, B.M.: Static and dynamic friction behavior of candidate high temperature airframe seal materials. (1994)
17. Coskun, M.B., Aksoy, S., Aksit, M.F.: Friction and wear characteristics of Haynes 25, 188, and 214 superalloys against Hastelloy X up to 540 °C. *Tribol. Lett.* **45**, 497–503 (2012)
18. Viat, A., Guillonneau, G., Fouvry, S., Kermouche, G., Sao Joao, S., Wehrs, J., Michler, J., Henne, J.F.: Brittle to ductile transition of tribomaterial in relation to wear response at high temperatures. *Wear* **392–393**, 60–68 (2017). <https://doi.org/10.1016/j.wear.2017.09.015>
19. Korashy, A., Attia, H., Thomson, V., Oskoeei, S.: Characterization of fretting wear of cobalt-based superalloys at high temperature for aero-engine combustor components. *Wear* **330**, 327–337 (2015)
20. Munagala, V.N.V., Alidokht, S.A., Sharifi, N., Makowiec, M.E., Stoyanov, P., Moreau, C., Chromik, R.R.: Room and elevated temperature sliding wear of high velocity oxy-fuel sprayed diamalloy3001 coatings. *Tribol. Int.* (2022). <https://doi.org/10.1016/j.triboint.2022.108069>
21. Scharf, T.W., Prasad, S.V., Kotula, P.G., Michael, J.R., Robino, C.: V: Elevated temperature tribology of cobalt and tantalum-based alloys. *Wear* **330**, 199–208 (2015)
22. Harrington, K.M., Miller, E.C., Frye, A., Stoyanov, P.: Tribological insights of Co- and Ni-based alloys in extreme conditions. *Wear* **477**, 203827 (2021)
23. Stott, F.H., Stevenson, C.W., Wood, G.C.: Friction and wear properties of Stellite 31 at temperatures from 293 to 1073K. *Met. Technol.* **4**, 66–74 (1977)
24. Stoyanov, P., Boyne, A., Ignatov, A.: Tribological characteristics of Co-based plasma sprayed coating in extreme conditions. *Results Surf. Interfaces* **3**, 100007 (2021)
25. Rynio, C., Hattendorf, H., Klöwer, J., Eggeler, G.: On the physical nature of tribolayers and wear debris after sliding wear in a superalloy/steel tribosystem at 25 and 300 °C. *Wear* **317**, 26–38 (2014)
26. Scharf, T.W., Prasad, S.V., Kotula, P.G., Michael, J.R., Robino, C.V.: Elevated temperature tribology of cobalt and tantalum-based alloys. *Wear* **330–331**, 199–208 (2015). <https://doi.org/10.1016/j.wear.2014.12.051>
27. Dreano, A., Fouvry, S., Sao-Joao, S., Galipaud, J., Guillonneau, G.: The formation of a cobalt-based glaze layer at high temperature: a layered structure. *Wear* **440–441**, 203101 (2019). <https://doi.org/10.1016/j.wear.2019.203101>
28. Laskowski, J.A., DellaCorte, C.: Friction and wear characteristics of candidate foil bearing materials from 25 °C to 800 °C. National Aeronautics and Space Administration, Washington (1996)
29. Peterson, M.B., Florek, J.J., Lee, R.E.: Sliding characteristics of metals at high temperatures. *ASLE Trans.* **3**, 101–109 (1960)
30. Patel, P., Alidokht, S.A., Sharifi, N., Roy, A., Harrington, K., Stoyanov, P., Chromik, R.R., Moreau, C.: Microstructural and tribological behavior of thermal spray CrMnFeCoNi high entropy alloy coatings. *J. Therm. Spray Technol.* (2022). <https://doi.org/10.1007/s11666-022-01350->
31. Darut, G., Ben-Ettouil, F., Denoirjean, A., Montavon, G., Ageorges, H., Fauchais, P.: Dry sliding behavior of sub-micrometer-sized suspension plasma sprayed ceramic oxide coatings. *J. Therm. Spray Technol.* **19**, 275–285 (2010). <https://doi.org/10.1007/s11666-009-9415-1>
32. Mohammadkhani, S., Jalilvand, V., Davis, B., Gauthier, G.H., Dolatabadi, A., Moreau, C., Roué, L., Guay, D.: High-temperature behaviour of HVOF (Co, Ni)O coated Cu–Ni–Fe anodes. *Corros. Sci.* **189**, 109563 (2021). <https://doi.org/10.1016/j.corsci.2021.109563>
33. Mohammadkhani, S., Jalilvand, V., Davis, B., Ettouil, F.B., Dolatabadi, A., Roué, L., Moreau, C., Guay, D.: Suspension plasma spray deposition of CoxNi_{1-x}O coatings. *Surf. Coatings Technol.* **399**, 126168 (2020). <https://doi.org/10.1016/j.surfcoat.2020.126168>
34. Tarasi, F., Medraj, M., Dolatabadi, A., Oberste-Berghaus, J., Moreau, C.: Enhancement of amorphous phase formation in alumina–YSZ coatings deposited by suspension plasma spray process. *Surf. Coatings Technol.* **220**, 191–198 (2013)
35. Roy, A., Munagala, V.N.V., Patel, P., Sharifi, N., Alidokht, S.A., Makowiec, M., Chromik, R.R., Moreau, C., Stoyanov, P.: Friction and wear behavior of suspension plasma sprayed tantalum oxide coatings at elevated temperatures. *Surf. Coatings Technol.* (2022). <https://doi.org/10.1016/j.surfcoat.2022.129097>
36. Roy, A., Sharifi, N., Munagala, V. N. V., Alidokht, S. A., Patel, P., Makowiec, M., Chromik, R. R., Moreau, C., Stoyanov, P.: Microstructural evolution and tribological behavior of suspension plasma sprayed CuO as high-temperature lubricious coatings. *Wear* (2022). <https://doi.org/10.1016/j.wear.2023.204874>
37. Küçük, Y.: Effect of counterbody on the dry sliding wear performance of plasma sprayed calcia-stabilized zirconia coating. *Int. J. Refract. Met. Hard Mater.* (2020). <https://doi.org/10.1016/j.ijrmhm.2020.105284>
38. Sabat, K.C.: Production of nickel by cold hydrogen plasma. *Plasma Chem. Plasma Process.* **41**, 1329–1345 (2021)
39. Sabat, K.C., Murphy, A.B.: Hydrogen plasma processing of iron ore. *Metall. Mater. Trans. B* **48**, 1561–1594 (2017)
40. Jalilvand, V., Mohammadkhani, S., Ettouil, F.B., Roué, L., Guay, D., Dolatabadi, A., Moreau, C.: Study on the formation of (Co, Ni) O solid solution and metallic Ni phases during suspension plasma spraying of CoO and NiO powders. *J. Therm. Spray Technol.* (2022). <https://doi.org/10.1007/s11666-022-01505-x>
41. Alidokht, S.A., Manimunda, P., Vo, P., Yue, S., Chromik, R.R.: Cold spray deposition of a Ni-WC composite coating and its dry sliding wear behavior. *Surf. Coatings Technol.* **308**, 424–434 (2016)
42. Swain, M.V.: Microscopic observations of abrasive wear of polycrystalline alumina. *Wear* **35**, 185–189 (1975)
43. Roro, K.T., Mwakikunga, B., Tile, N., Yalisi, B., Forbes, A.: Effect of accelerated thermal ageing on the selective solar thermal

- harvesting properties of multiwall carbon nanotube/nickel oxide nanocomposite coatings. *Int. J. Photoenergy*. (2012). <https://doi.org/10.1155/2012/678394>
44. Korashy, A., Attia, H., Thomson, V., Oskooei, S.: Characterization of fretting wear of cobalt-based superalloys at high temperature for aero-engine combustor components. *Wear* **330–331**, 327–337 (2015). <https://doi.org/10.1016/j.wear.2014.11.027>
 45. Yao, Q., Jia, J., Chen, T., Xin, H., Shi, Y., He, N., Feng, X., Shi, P., Lu, C.: High temperature tribological behaviors and wear mechanisms of NiAl-MoO₃/CuO composite coatings. *Surf. Coatings Technol.* **395**, 125910 (2020)
 46. Chromik, R.R., Zhang, Y.: Nanomechanical testing of third bodies. *Curr. Opin. Solid State Mater. Sci.* **22**, 142–155 (2018)
 47. Goel, S., Björklund, S., Curry, N., Wiklund, U., Joshi, S.V.: Axial suspension plasma spraying of Al₂O₃ coatings for superior tribological properties. *Surf. Coatings Technol.* **315**, 80–87 (2017). <https://doi.org/10.1016/j.surfcoat.2017.02.025>
 48. Mahade, S., Mulone, A., Björklund, S., Klement, U., Joshi, S.: Incorporation of graphene nano platelets in suspension plasma sprayed alumina coatings for improved tribological properties. *Appl. Surf. Sci.* **570**, 151227 (2021)
 49. Erickson, L.C., Blomberg, A., Hogmark, S., Bratthäll, J.: Tribological characterization of alumina and silicon carbide under lubricated sliding. *Tribol. Int.* **26**, 83–92 (1993)
 50. Stachowiak, G.W., Batchelor, A.W.: *Engineering tribology*. Butterworth-heinemann (2013)
 51. Watanabe, H.: Thermal constants for Ni, NiO, MgO, MnO and CoO at low temperatures. *Thermochim. Acta.* **218**, 365–372 (1993)
 52. Rynio, C., Hattendorf, H., Klöwer, J., Eggeler, G.: The evolution of tribolayers during high temperature sliding wear. *Wear* **315**, 1–10 (2014)
 53. Shakhvorostov, D., Gleising, B., Büscher, R., Dudzinski, W., Fischer, A., Scherge, M.: Microstructure of tribologically induced nanolayers produced at ultra-low wear rates. *Wear* **263**, 1259–1265 (2007)
 54. Greiner, C., Liu, Z., Strassberger, L., Gumbsch, P.: Sequence of stages in the microstructure evolution in copper under mild reciprocating tribological loading. *ACS Appl. Mater. Interfaces.* **8**, 15809–15819 (2016)
 55. Bowden, F.P., Bowden, F.P., Tabor, D.: *The friction and lubrication of solids*. Oxford university press (2001)
 56. Tang, C.-W., Wang, C.-B., Chien, S.-H.: Characterization of cobalt oxides studied by FT-IR, Raman TPR and TG-MS. *Thermochim. Acta.* **473**, 68–73 (2008)
 57. Nicholls, J.R., Hall, D.J., Tortorelli, P.F.: Hardness and modulus measurements on oxide scales. *Mater. High Temp.* **12**, 141–150 (1994)
 58. Archard, J.: Contact and rubbing of flat surfaces. *J. Appl. Phys.* **24**, 981–988 (1953)
 59. Muratore, C., Voevodin, A.A.: Chameleon coatings: adaptive surfaces to reduce friction and wear in extreme environments. *Annu. Rev. Mater. Res.* **39**, 297–324 (2009)
 60. Mokhtar, M.O.A.: The effect of hardness on the frictional behaviour of metals. *Wear* **78**, 297–304 (1982)
 61. Schulz, H., Dörr, J., Rass, I.J., Schulze, M., Leyendecker, T., Erkens, G.: Performance of oxide PVD-coatings in dry cutting operations. *Surf. Coatings Technol.* **146**, 480–485 (2001)
 62. Moore, A.J.W., Tegart, W.J.M.: Relation between friction and hardness. *Proc. R. Soc. London. Ser. A. Math. Phys. Sci.* **212**, 452–458 (1952)
 63. Evans, A.G., Rajdev, D., Douglass, D.L.: The mechanical properties of nickel oxide and their relationship to the morphology of thick oxide scales formed on nickel. *Oxid. Met.* **4**, 151–170 (1972)
 64. Dimitrov, V., Komatsu, T.: Classification of simple oxides: a polarizability approach. *J. Solid State Chem.* **163**, 100–112 (2002)
 65. Prakash, B., Celis, J.P.: The lubricity of oxides revised based on a polarisability approach. *Tribol. Lett.* **27**, 105–112 (2007). <https://doi.org/10.1007/s11249-007-9223-z>

Publisher's Note Springer Nature remains neutral with regard to jurisdictional claims in published maps and institutional affiliations.

Springer Nature or its licensor (e.g. a society or other partner) holds exclusive rights to this article under a publishing agreement with the author(s) or other rightsholder(s); author self-archiving of the accepted manuscript version of this article is solely governed by the terms of such publishing agreement and applicable law.